Article

Cell Systems

A Local, Self-Organizing Reaction-Diffusion Model Can Explain Somite Patterning in Embryos

Graphical Abstract

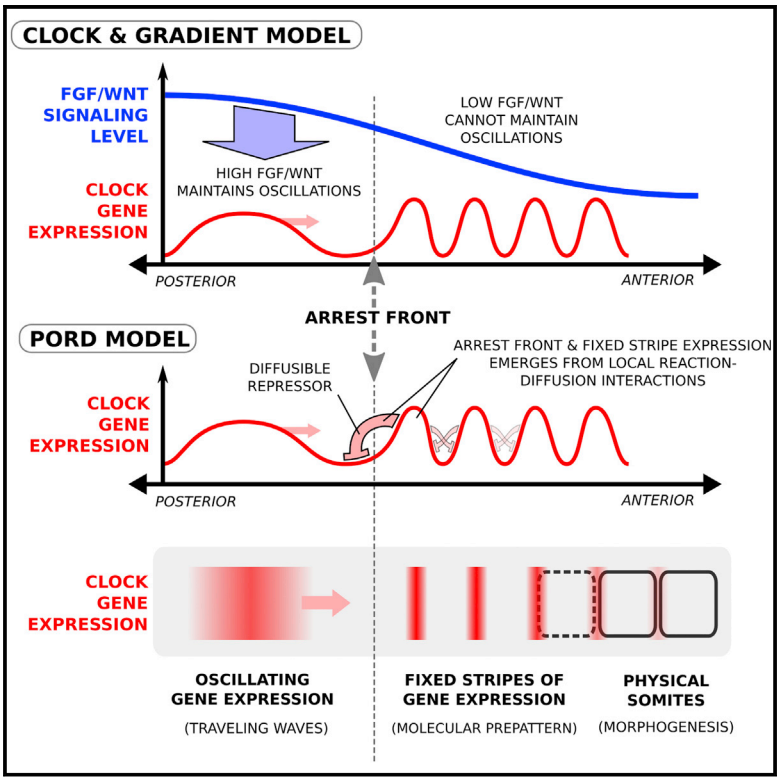

Highlights

- A systematic computational screen identifies networks based on behavior
- Computation shows that somitogenesis can be explained by short-range interactions
- Short-range and long-range models are tested head-to-head in silico and in vivo
- Short-range models explain aspects of somitogenesis that previous models cannot

Authors

James Cotterell,
Alexandre Robert-Moreno,
James Sharpe

Correspondence

j.cotterell@garvan.org.au (J.C.),
james.sharpe@crg.es (J.S.)

In Brief

Using a systematic computational approach and in vivo experiments, Cotterell et al. challenge a 40-year-old model that explains large-scale embryonic patterns in terms of long-range gradients. Instead, they show that these patterns can arise from short-range interactions and that a modified reaction-diffusion mechanism can drive the self-organization observed during somitogenesis.

Cotterell et al., 2015, Cell Systems *1*, 257–269
October 28, 2015
http://dx.doi.org/10.1016/j.cels.2015.10.002

CellPress

Cell Systems
Article

A Local, Self-Organizing Reaction-Diffusion Model Can Explain Somite Patterning in Embryos

James Cotterell,[1,2,*] Alexandre Robert-Moreno,[1,2] and James Sharpe[1,2,3,*]
[1]EMBL-CRG Systems Biology Research Unit, Centre for Genomic Regulation (CRG), The Barcelona Institute of Science and Technology, Dr. Aiguader 88, Barcelona 08003, Spain
[2]Universitat Pompeu Fabra (UPF), Barcelona 08002, Spain
[3]Institució Catalana de Recerca i Estudis Avançats (ICREA), Pg. Lluís Companys 23, 08010 Barcelona, Spain
*Correspondence: j.cotterell@garvan.org.au (J.C.), james.sharpe@crg.es (J.S.)
http://dx.doi.org/10.1016/j.cels.2015.10.002

SUMMARY

During somitogenesis in embryos, a posteriorly moving differentiation front arrests the oscillations of "segmentation clock" genes, leaving behind a frozen, periodic pattern of expression stripes. Both mathematical theories and experimental observations have invoked a "clock and wavefront" model to explain this phenomenon, in which long-range molecular gradients control the movement of the front and therefore the placement of the stripes in the embryo. Here, we develop a fundamentally different model—a progressive oscillatory reaction-diffusion (PORD) system driven by short-range interactions. In this model, posterior movement of the front is a local, emergent phenomenon that, in contrast to the clock and wavefront model, is not controlled by global positional information. The PORD model explains important features of somitogenesis, such as size regulation, that previous reaction-diffusion models could not explain. Moreover, the PORD and clock and wavefront models make different predictions about the results of FGF-inhibition and tissue-cutting experiments, and we demonstrate that the results of these experiments favor the PORD model.

INTRODUCTION

During the development of all vertebrate embryos, the presomitic mesoderm (PSM), which lies on either side of the neural tube, is progressively segmented from anterior to posterior (from approximately day 1 to day 3 in the chick embryo) into a series of transient epithelial balls called somites, which later give rise to vertebrae, muscle blocks, and skin. This physical "budding" process is prefigured by a molecular patterning process that sequentially produces stripes of gene expression along the PSM, again in an anterior-to-posterior sequence (for example *Lfng*); each stripe of expression will, in future, correspond to a subsequent somite boundary. The control of this molecular segmentation process has been a paradigmatic example of pattern formation for the last 50 years and as such has a long conceptual history of proposed underlying mechanisms (Kulesa et al., 2007). These expression stripes are very regular in size and are widely believed to result from the interaction of two dynamical systems. First, cells of the PSM exhibit oscillations of gene expression—mostly components of the Notch signaling pathway (Palmeirim et al., 1997; Forsberg et al., 1998; McGrew et al., 1998; Aulehla and Johnson 1999; Holley et al., 2000; Jouve et al., 2000; Jiang et al., 2000; Sawada et al., 2000; Bessho et al., 2001a, 2001b; Oates and Ho, 2002). Along the PSM, these oscillations are spatially organized into traveling waves, but this feature is not important for the questions or models discussed here. The important feature is that the oscillations are locally well synchronized: neighboring cells are in very similar phases of the cycle. Second, these oscillations are arrested in an anterior-to-posterior progression. The position where oscillations are frozen travels posteriorly through the PSM (thus prefiguring the progression of morphological segmentation itself). This traveling position is called the arrest front (Herrgen et al., 2010). It is widely believed that the moment when cells stop oscillating is when their fate has become committed to a given part of a presumptive somite. The progressive freezing of the oscillations effectively transforms a temporal oscillation into a spatial periodicity. (The distinction between the definitions of the *arrest front* and the *determination front* is addressed in the discussion below).

Our study focuses on how the posterior movement of the arrest front is controlled (rather than the oscillations). Currently prevailing models to explain the arrest front focus on large-scale morphogen gradients. Both FGF and WNT signaling display long spatial gradients with highest levels observed in the embryo's posterior (Dubrulle et al., 2001; Dubrulle and Pourquié, 2004; Sawada et al., 2001; Aulehla et al., 2003). As the tailbud elongates due to growth, the gradients travel posteriorly through the PSM (probably involving progressive decay of mRNA rather than diffusion; Dubrulle and Pourquié, 2004) and a given signaling intensity therefore moves at the same velocity as overall growth of the tissue (Figure 1A). Because molecular oscillations are only seen posteriorly to the arrest front, it is proposed that morphogen signaling has the role of maintaining the oscillations and that arrest occurs once signaling drops below a certain level. Support for this idea has come from experimentally inhibiting and enhancing FGF signaling, both globally and locally, resulting in somite size changes that are consistent with this hypothesis (Dubrulle et al., 2001; Sawada et al., 2001; Naiche et al., 2011). For example, a sudden but transient global reduction in FGF signaling (using the inhibitor SU5402)

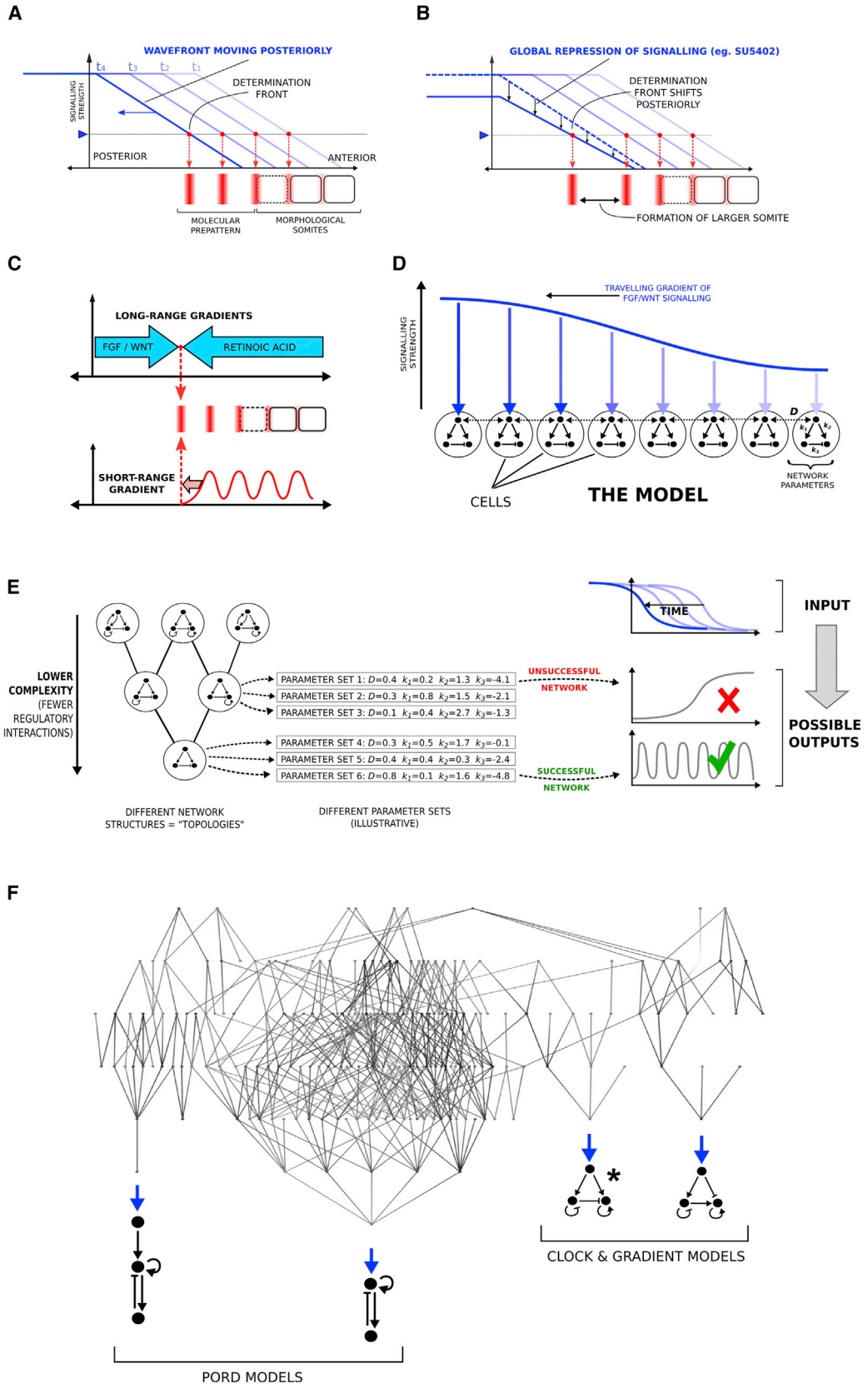

(legend on next page)

results in the formation of a single large somite, followed by normal sized somites (Dubrulle et al., 2001). This can be explained because a sudden global repression of a long spatial gradient would result in an effective posterior jump in signaling levels, causing a sudden but transient increase in wavefront velocity (see Figure 1B). In addition to experimental evidence, the majority of computational models have also supported this hypothesis (Baker et al., 2006a, 2006b; François et al., 2007; Hester et al., 2011; Tiedemann et al., 2012). In all of these cases, the wavefront was implemented as an effective threshold level of a posteriorly moving morphogen gradient, so we shall call this prevailing type of model the clock and gradient (C&G) model.

This much-studied C&G model corresponds only to the first of two broad categories of model considered by Cooke and Zeeman (1976) in their seminal paper from 1976. This first category was named as the clock and wavefront model, and it proposed that the position of the posteriorly traveling arrest front is defined with respect to the whole PSM. In other words, some mechanism exists to provide positional information along the PSM, and this mechanism is used to determine where the arrest front is at any moment in time. In all the literature cited above, this mechanism is hypothesized to be the large-scale molecular gradients, which translate posteriorly through the PSM as it grows.

However, Cooke and Zeeman (1976) also considered a second category of model, based on local self-organization rather than global positional information. Although it failed to gain the traction that the C&G model has appreciated, this category of model, based on a Turing-type reaction-diffusion (RD) mechanism, can produce exactly the kind of repeated periodic patterns seen in somite patterning. These RD models represent a genuine alternative concept, as they do not rely on long-range information (e.g., morphogen gradients), but instead only on local interactions. The two categories of model thus present a genuine dichotomy, which was indeed emphasized by Cooke and Zeeman (1976) when promoting their clock and wavefront model: "We stress the necessary relation between the present model and the more general concept of positional information." The second category of self-organizing models was rejected due to the observed scaling of somites when embryo size is manipulated (Cooke, 1975). Turing systems that dynamically couple their wavelength to tissue size (Ishihara and Kaneko, 2006) were unknown at the time. The clock and wavefront model was thus the stronger explanation at the time, and almost all experimental observations since then have been interpreted in this light, leading to the more specific and current C&G models.

Despite the apparent success and popularity of the C&G model, we chose to revisit the relative merits of the two categories of model through an unbiased, systems biology approach that combines computational modeling with experimental testing of the theoretical predictions. Using this approach, we show that a model, which we call the progressive oscillatory reaction-diffusion (PORD) model, can also explain all known observations regarding the sequential periodic process of somite patterning. Despite being a local self-organizing model, it does involve both molecular oscillations in the PSM and a traveling wavefront. Nevertheless, it does not correspond to a clock and wavefront model, and crucially, it continues to make stripes even in the absence of a moving FGF/WNT gradient. Thus it does not rely on positional information along the PSM. In our RD model, the distance between stripes is defined by the local diffusion of a repressor molecule, which is secreted from the stripes themselves (Figure 1C). We here show that our RD model can explain somite size scaling, higher robustness of somite size regulation (compared with C&G), and the results of most published perturbation experiments. Our theoretical analysis also makes a number of testable predictions, which we test in chick embryos, head to head against the C&G model. In particular, we show experimental evidence that decouples the global Fibroblast Growth Factor (FGF)/WNT morphogen gradients from the arrest front. Our results revive a fundamentally alternative theory based on local self organization, last proposed 39 years ago, and challenge both the prevailing C&G model and the more general clock and wavefront model.

Figure 1. Models of Somite Patterning

(A) The C&G hypothesis in a WT context. The strength of FGF/WNT signaling (y axis) is distributed as a monotonically decreasing gradient (blue diagonal line) along the primary axis of the PSM (x axis). The gradient moves posteriorly over time (as indicated by the time points t_1 to t_4). A certain level of signaling (blue arrowhead) specifies the position of the arrest front. At periodic intervals (determined by oscillations of the clock genes), the current position of the arrest front (red dots) determines the formation of the next molecular prepattern stripe for somite boundary formation.

(B) Rapid global repression of wavefront signaling causes an effective posterior shift of signaling levels and thus a rapid shift of the arrest front, creating a larger somite. The signaling gradient is shown as a linear gradient here, but the hypothesis does not depend on the detailed shape of the gradient nor on whether it is formed by diffusion, cell-cell signaling, or cell-autonomous differential decay, as suggested by Dubrulle and Pourquié (2004).

(C) The positional accuracy of the arrest front will be more sensitive to noise if defined by long-range gradients (top) than if defined by the distance from the last-formed expression stripe (bottom).

(D) Our modeling framework consists of a row of virtual cells, each containing a simple gene regulatory network (GRN), which has a regulatory input from the posteriorly moving global signaling gradient (vertical blue arrows). Local cell-cell communication is abstracted as a simple diffusion process, and each model depends on parameters defining both the strengths and signs of regulatory interactions (k_1, k_2, k_3), and the effective diffusion constant of signaling molecules (D).

(E) The exhaustive list of GRN topologies is organized into a complexity atlas, in which network designs are represented as connected nodes if they differ by the addition or removal or just one regulatory link. Simpler networks (fewer regulatory interactions) are placed lower in the atlas. Simulating these hypothetical networks involves choosing random parameter values. Many different parameter sets (up to 1 million) were tested for each topology. The objective function takes the posteriorly traveling global gradient as its input (FGF/WNT) and tests whether each hypothetical network is successful at producing a spatially periodic pattern of gene expression or not.

(F) The resulting complexity atlas shows that successful networks are grouped into "stalactites" (Cotterell and Sharpe, 2010) in which the minimal version of the network design is the lowest point of the stalactite. Two small stalactites are found containing networks which operate by the C&G hypothesis; indeed, one of these core topologies (asterisk) has the exact same wiring diagram as the model found by François et al. (2007). However, a far greater number of successful networks fall into another stalactite which function by the PORD mechanism.

RESULTS

Unbiased Exploration of Network Design Space Reveals a Model for Progressive Somite Patterning Based on Local Self-Organization

We recently developed an approach to explore the mechanistic possibilities that can underlie morphogen interpretation (Cotterell and Sharpe, 2010). In this method, we enumerate all network designs (topologies) that are possible for a gene regulatory network of three genes. We simulate each of these topologies (nearly 10,000) in a 1D row of virtual cells to explore which spatial gene expression patterns they are capable of producing (Figure 1D). Gene levels are continuous variables, and their dynamics depend on the following model parameters: the strength and sign of the interactions between genes, degradation rates, and also on cell-cell communication, which is represented by a diffusive process (see Supplemental Experimental Procedures for more details). We add a stochastic noise term into the model, as our goal is to find networks that are robust to stochastic molecular noise. This term represents temporal fluctuations of molecular concentrations and produces gene expression variability comparable to that seen in real patterning systems (Cotterell and Sharpe, 2010). Networks are considered functional only if they repeatedly produce the same pattern despite being exposed to different sequences of stochastic fluctuations. In applying this approach to somite patterning, we added a couple of extra features: the morphogen input function was a moving gradient, rather than a static one, to represent the posteriorly moving FGF/WNT gradients, and we added the possibility of explicit time delays in the gene regulatory function to allow a richer collection of possible network dynamics. Each topology is simulated up to 1,000,000 times with random parameter values to explore parameter space in an unbiased way (see Supplemental Experimental Procedures for more details). This is an important departure from previous studies (François et al., 2007), which used in silico evolution, which tries to focus in on more successful regions of parameter space.

To test these millions of randomly sampled networks, we devised a flexible description of the multi-stripe pattern that should be achieved that had no constraints on the position or widths of the stripes (Supplemental Experimental Procedures). All three genes in the network were assessed, and a successful pattern must be reproducible in the face of different sequences of stochastic noise. Of the 9,710 topolgies analyzed, 210 produced a multi-stripe pattern for at least one parameter set. Exploring the dynamic mechanism of so many networks is a non-trivial task, and thus we chose to employ our ''complexity atlas'' approach (Cotterell and Sharpe, 2010), which helps to reveal the main groups of alternative dynamical mechanisms. Each successful topology is considered to be a node in a larger non-directed graph (see Figure 1E). Pairs of topologies are directly linked if they display only one topological difference between them (i.e., the addition or removal of a single gene-gene regulatory interaction). The resulting metagraph (graph of graphs) is then spatially arranged such that the simplest topologies are placed at the bottom (i.e., topologies with fewest regulatory interactions) and the most complex networks at the top (see Figure 1E). This arrangement has the advantage of directly revealing potentially alternative network mechanisms as ''stalactites.'' Different topologies within the same stalactite tend to function with the same dynamics, while topologies located in different stalactites are likely to function in a qualitatively distinct manner.

Examination of the complexity atlas for somite patterning (Figure 1F) revealed a few small stalactites accounting for only 14% of the topologies, plus one predominant stalactite containing the majority of successful topologies. Two of the minimal designs are indeed versions of the popular C&G model—in other words, the global morphogen gradient maintains oscillations in the posterior PSM and its posterior movement thus directly drives the arrest front (as cells lose a sufficient signaling level their oscillations freeze and a spatial periodic pattern is left behind). In these cases, as expected, somite size is always a function of the oscillatory period at the arrest front (***p***) and velocity of the arrest front (***v***). Unsurprisingly, one of these minimal C&G networks has the exact same design as the model found by François et al. (2007) by in silico evolution, which was also understood to function as a standard C&G model (see Movie S1).

When we analyzed the dynamics and behavior of networks in the large stalactite, we found that they operate in a fundamentally different way from the C&G model and were also far more robust to stochastic noise (Figures 2 and S1). The simplest version of our mechanism is a network of only two nodes (Figure 2A), comprising a cell-autonomous activator (*A*), which is itself activated by the FGF signal, and a diffusible repressor (*R*), whose levels are defined by the following equations:

$$\frac{\partial A}{dt} = \Phi\left(\frac{k_1 A - k_2 R + F + \beta}{1 + k_1 A - k_2 R + F + \beta}\right) - \mu A \qquad \text{(Equation 1)}$$

$$\frac{\partial R}{dt} = \frac{k_3 A}{1 + k_3 A} + D\nabla^2 R - \mu R, \qquad \text{(Equation 2)}$$

where k_1, k_2, and k_3 define the strengths of regulatory interactions between *A* and *R*, *D* is the diffusion constant for *R*, μ is a fixed decay constant, and *F* is the regulatory input of the FGF/WNT gradient onto *A*. β is the background regulatory input of A (the gene receiving the morphogen activation). To prevent negative values, we use the function $\Phi(x) = x.H(x)$, where H(x) is the standard Heaviside function (H(x) = 1 for $x > 0$ and H(x) = 0 for $x < 0$). Together, *A* and *R* form a RD mechanism in which lateral inhibition is responsible for the regular spacing of adjacent expression stripes. Our model does not spontaneously generate segments everywhere (Turing, 1952; Kondo and Miura, 2010), but rather progresses from anterior to posterior, mimicking the normal process of somite formation. Simulated PSM cells display oscillations of gene expression, which are spatially organized into traveling waves (see Movies S2 and S3). These are initiated at the growing tail bud, where FGF levels are highest, and propagate anteriorly until they narrow and freeze into a stable fixed stripe of expression several cell diameters away from the previously formed stripe (Figure 2B). Parameter values, model configurations, and simulation results for all models discussed in this paper are presented in the Simulation Sheets in the Supplemental Information. We name our system the PORD model and note that it is not equivalent to a model previously proposed by Meinhardt (1982), which involves two

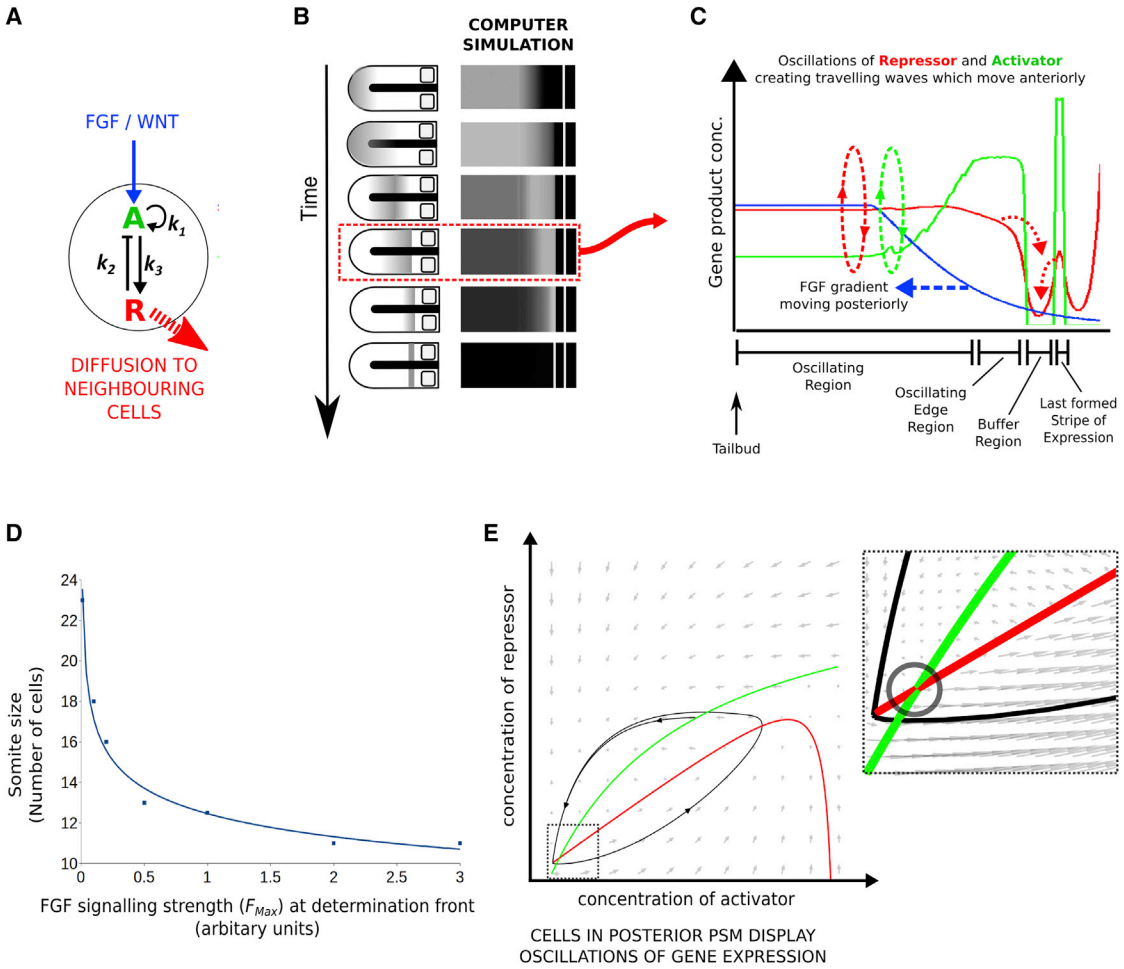

Figure 2. The PORD Mechanism

(A) The minimal somite-patterning circuit found in our study, which implements the PORD mechanism, comprises an activator molecule (green) and a diffusible repressor (red). This same three-color code (blue for the global gradient input) is used throughout the subsequent figures and Supplemental Movies.

(B) The PORD mechanism produces waves of gene expression that initiate at the posterior end of the embryo and travel anteriorly. The waves thin and slow as they reach the last formed expression stripe. Parameter values and other details for all simulations are given in the Supplemental Methods.

(C) A snapshot of gene levels along the PSM according to the PORD model. Oscillations of activator and repressor are indicated by the oval dashed arrows. The FGF/WNT gradient is shown (blue) but is not necessary for stripe formation. The buffer region is generated by diffusion of repressor from the last formed somite boundary posteriorly (dotted red arrow), which inhibits oscillations. In the oscillating edge region, cells can exit oscillations to form a stripe of gene expression by alleviation of repression due to diffusion of repressor into the buffer region (red dotted arrow). For each cycle of oscillations, a new group of cells at the oscillating edge exits cycling and forms a new stripe. These cells thus act as the next source of repressor to prevent oscillations more caudally and push the arrest front caudally.

(D) Plotting segment size against total integral FGF signaling strength in the PSM demonstrates that the PORD model is capable of size regulation if embryo growth is assumed to dilute the amount of FGF signaling in the PSM. A higher growth rate would cause greater dilution of the FGF signal causing larger somites in the PORD model.

(E) The phase portrait for the non-diffusing case of Equations (1) and (2), without Φ, reveals that oscillations are the natural dynamic state for most cells in the PSM (due to the negative feedback in the circuit). The nullclines for the activator and inhibitor are shown as green and red lines, respectively (equations given in Supplemental Methods).

mutually repressing cellular states, rather than an activator-inhibitor mechanism.

In our PORD model, arrest of the "clock" is not caused by the posteriorly traveling long-range signaling gradient, but rather by the short-range repressor *R*, which diffuses from the last-formed stripe. This creates a "buffer region," which prevents the next anteriorly traveling wave of gene expression from getting too close to the last-formed stripe (Figure 2C). It also allows repressor to diffuse anteriorly from the edge of the oscillatory region lowering its level and allowing the activator to self-enhance up to a new stable stripe of expression. In fact we find that a posteriorly traveling FGF/WNT gradient is not required for the functionality of the PORD model at all. Unlike the C&G model, our PORD model can still work with a completely flat spatial distribution, or a non-moving gradient of FGF/WNT signaling (Figure S2; see Movie S4). The posteriorly moving arrest front is an emergent phenomenon from the local RD interactions of cells—it is not directly coupled to (or dependent on) the posteriorly moving

gradients of FGF signaling. More generally, it is not dependent on any form of long-range positional information along the PSM, thus distinguishing itself also from the more general clock and wavefront model. Furthermore, we explored the parameter requirements of the PORD model and found that they lie within physiological relevant ranges (Figure S3). These and all further comparisons between the PORD and C&G models are detailed side-by-side in the ''Simulation Sheets'' included in the Supplemental Information, including all parameter values used.

It is important to note that our PORD model does not challenge the known relationship between somite size (***s***), oscillatory period at the arrest front (***p***), and velocity of the arrest front (***v***). The equality ***s*** = ***p.v*** is necessarily true by definition; it does not per se distinguish between different possible mechanisms. However, the PORD model makes a different prediction from the C&G model about causality—about which variable is a function of the others. While the C&G model proposes that somite size is a function of period and velocity (***s*** = *f*(***p***,***v***), *specifically* ***s*** = ***p***.***v***), our PORD model proposes that it is ***s*** and ***p*** that are given (somite size is determined by the diffusible repressor, and period is determined by the dynamics of the negative feedback), and it is ***v*** which is an emergent consequence of these intrinsic values; i.e., ***v*** = *f*(***s***,***p***), specifically ***v*** = ***s***/***p***.

Two previous criticisms have been made against RD models for somite patterning. First, somites scale with body size (Cooke, 1975), which is hard to explain by a classical Turing model. Here we show that in the PORD mechanism FGF signaling counterbalances the effects of the local diffusible repressor; thus, higher levels of FGF signaling result in smaller somites (Figure 2D). Hence, although the moving FGF gradient is not required for somitogenesis per se, it nevertheless acts to couple the rate of embryo growth with the integral levels of FGF signaling in the PSM. A faster growing tissue dilutes the FGF signal and results in larger somites (as the local repressor creates a larger buffer zone). Second, although a consensus view has not yet been reached on whether such cell-autonomous oscillations exist, evidence in favor has been reported (Jiang et al., 2000; Maroto et al., 2005), and this would not occur in a traditional Turing model. However, examining the phase portrait of the non-diffusing case of Equations (1) and (2) (i.e., *D* set to zero) reveals that our PORD model naturally undergoes oscillations in the absence of diffusion (explained in Figure 2E).

Restarting the Relay with a Cut in the PSM

A clear prediction of our PORD model is that the posteriorly traveling arrest front is a propagatory wave, thus dependent on the local cell-cell communication of the RD system. Certain classic tissue manipulation experiments, in which PSM of early chick embryos was explanted and/or grafted, seem to dispute this (Deuchar and Burgess, 1967; Pearson and Elsdale, 1979; Packard and Jacobson, 1976; Packard, 1978). For example, if posterior PSM is isolated from anterior tissue, it will continue generating somites. Such observations have been considered as evidence against a propagatory wave of patterning in the PSM since there would be no way for anterior tissue to communicate with posterior tissue across the cut. They supported instead a kinematic wave hypothesis, in which earlier patterning events (such as molecular gradients) give positional information to each cell in the PSM and the ''memory'' of this allows cells to subsequently undergo a progressive anterior-to-posterior sequence of patterning in a completely cell-autonomous manner which follows the normal timing.

How can the results of PSM cut experiments be reconciled with a patterning mechanism based on a progressive relay signal? As we have seen above, in the PORD model, oscillations are stopped in the buffer zone by repressor levels, which have diffused out from the last-formed stripe (Figure 2C). However, our theoretical exploration of the PORD model also revealed a second mode of stopping the clock. If FGF signaling is increased dramatically cells also stop oscillating and expression levels of the activator reach a high stable state (as in the normal stripe cells). Wound healing responses have been studied for many years, and it has been demonstrated that FGF signaling is essential in regeneration of both the *Xenopus* tadpole tail and zebrafish fins (Whitehead et al., 2005; Lin and Slack, 2008). Hence, we postulated that a cut in the PSM might induce FGF signaling through a wound response. To test this idea, we cut the PSM of HH9-12 chick embryos at a position that is 4 somite lengths posterior of the currently forming somite (known as position −IV) and monitored the distribution of double-phosphorylated ERK—a molecular readout of FGF signaling—at different time points during ex ovo incubation. Indeed, we find that ERK signaling is upregulated at the cut site within a few hours (Figure 3A), which prompts the need to re-evaluate the conclusions of previously published PSM-cut experiments. Our data suggest that in all previous PSM-cut experiments the ERK-mediated wound response will have been triggered and that this could have acted as a direct inducer of a new stripe of boundary gene expression. Computer simulations of the PORD model within this scenario show that reproducing this abnormal FGF signaling on the edge of the cut tissue (quantified using dpERK signal; Figure 3B) is sufficient to re-start the relay process, i.e., re-starting the progressive posterior-wards patterning of somites (Movie S5). We therefore conclude that the results of previous PSM-cutting experiments do not rule out a relay-type of model for somite patterning.

The observations suggest a critical possibility: that it may be possible to decouple the determination front from the FGF signaling gradient, thus questioning the role of global positional information. In the next section, we show that it is possible to alter the position where stripes are being formed without shifting the position of the FGF signaling gradient, and in the subsequent section, we show the inverse—that the FGF signaling gradient can be shifted without the determination front following it.

Decoupling the Determination Front from the FGF Signaling Gradients

To explore the first possibility, we performed straight cuts across the PSM at position -VIII and then performed double in situ hybridizations to simultaneously monitor the position of the long-range signaling front and the position where the next molecular stripe was being formed. Very few molecular readouts of FGF/WNT signaling show a measurable sharp axial boundary in the PSM, but *Msgn1*, a downstream target of WNT signaling, has been used as a suitable readout of the determination front (Gomez et al., 2008). We thus used probes for *Msgn1* (as a readout of the signaling front position) and *Lfng* (as a readout out of stripe formation) at fixed time intervals after cutting.

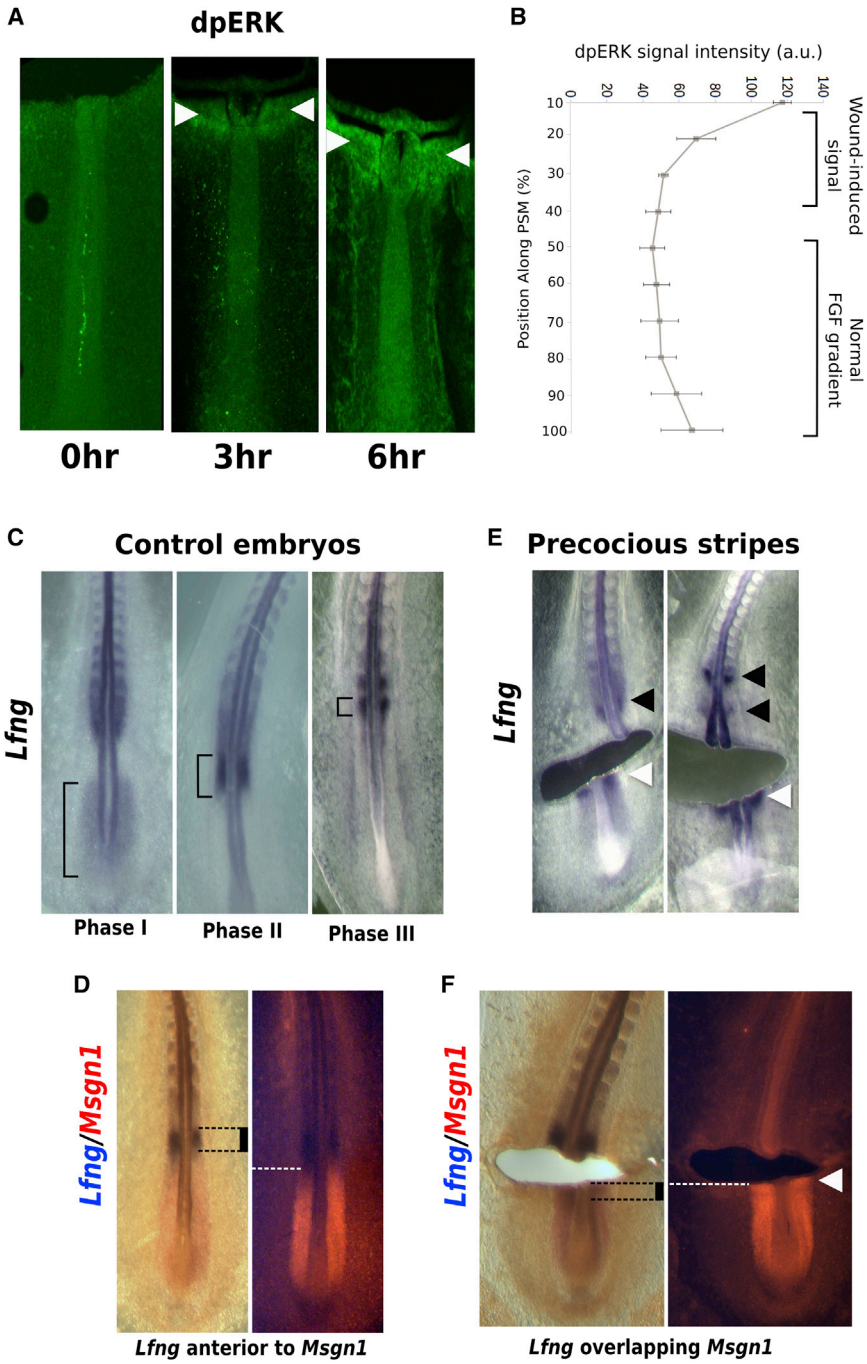

Figure 3. Decoupling the Progression of Segmental Patterning from the Progression of Global Gradients by Straight PSM Cuts

(A) Whole-mount immunohistochemistry at 0-, 3-, and 6-hr incubation ex ovo after a straight cut, showing that dpERK is reactivated at the cut edge (white arrowheads).

(B) Quantification of double-phosphorylated ERK (dpERK) levels over the PSMs of cut embryos at the 6-hr time point. The results are split into ten percentile bins with SE plotted (n = 3).

(C) Control embryos display the characteristic three phases of lunatic fringe expression.

(D) In control embryos, phase III lunatic fringe expression is anterior to the domain of expression of *Msgn1*.

(E) Precocious stripes of lunatic fringe expression are observed posteriorly and adjacent to a cut at position −VIII after 8 hr of incubation (n = 10/31). Precocious stripes are indicated by white arrowheads, and normal stripes are indicated by black arrowheads.

(F) In cut embryos the precocious stripe of lunatic fringe is within the *Msgn1* expressing domain (n = 15/15 for observed precocious stripes). Ectopic *Msgn1* expression next to the cut (induced by dpERK) is sometimes observed (white arrowhead).

Control embryos demonstrate well-defined waves of *Lfng* gene expression collapsing into well-defined stripes of gene expression in the anterior PSM (Figure 3C). The three distinct phases of *Lfng* oscillation can be seen. In these embryos, the phase II wave or final phase III stripe of *Lfng* is always anterior to the domain of *Msgn1* expression (Figure 3D). When we cut the embryo, however, after 6 hr, an extra precocious stripe of *Lfng* gene expression has formed on the posterior edge of the cut (n = 10/31; white arrowheads in Figure 3E). The normal stripe of expression can also be seen in its usual position in the anterior PSM in the same embryos and occasionally a third stripe (black arrowheads in Figure 3E), which highlights how posterior and precocious the extra stripes are. It is also evident that the precocious stripe is within the extended domain of Msgn1 (Figure 3F) in contrast to the normal situation where it is anterior to this domain (Figure 3D). A decoupling of stripe formation from the long-range gradients has therefore been observed, which contradicts the C&G model, but this can be explained by the PORD model as a consequence of the upregulation of ERK signaling (Figure 3A).

The observation of restarting the relay with a cut across the PSM makes a second important prediction. Somite boundaries and stripes of gene expression should always occur next to a cut site—at a fixed, small distance indicating control by the cut rather than by the global signaling gradients. To test this possibility, we performed a simple experiment that supports either the C&G or PORD mechanisms: cutting the PSM diagonally. We performed diagonal cuts across the PSM with approximately a half somite difference in position on either side of the embryo. These diagonal cuts were performed at various positions between −IV and −VIII. The postulated "determination front" should be anterior to the cut, and in an 8-hr time window, we can observe the effects as it passes through the cut site. The C&G and the PORD mechanism make qualitatively different predictions about the spatial arrangement of expression stripes when

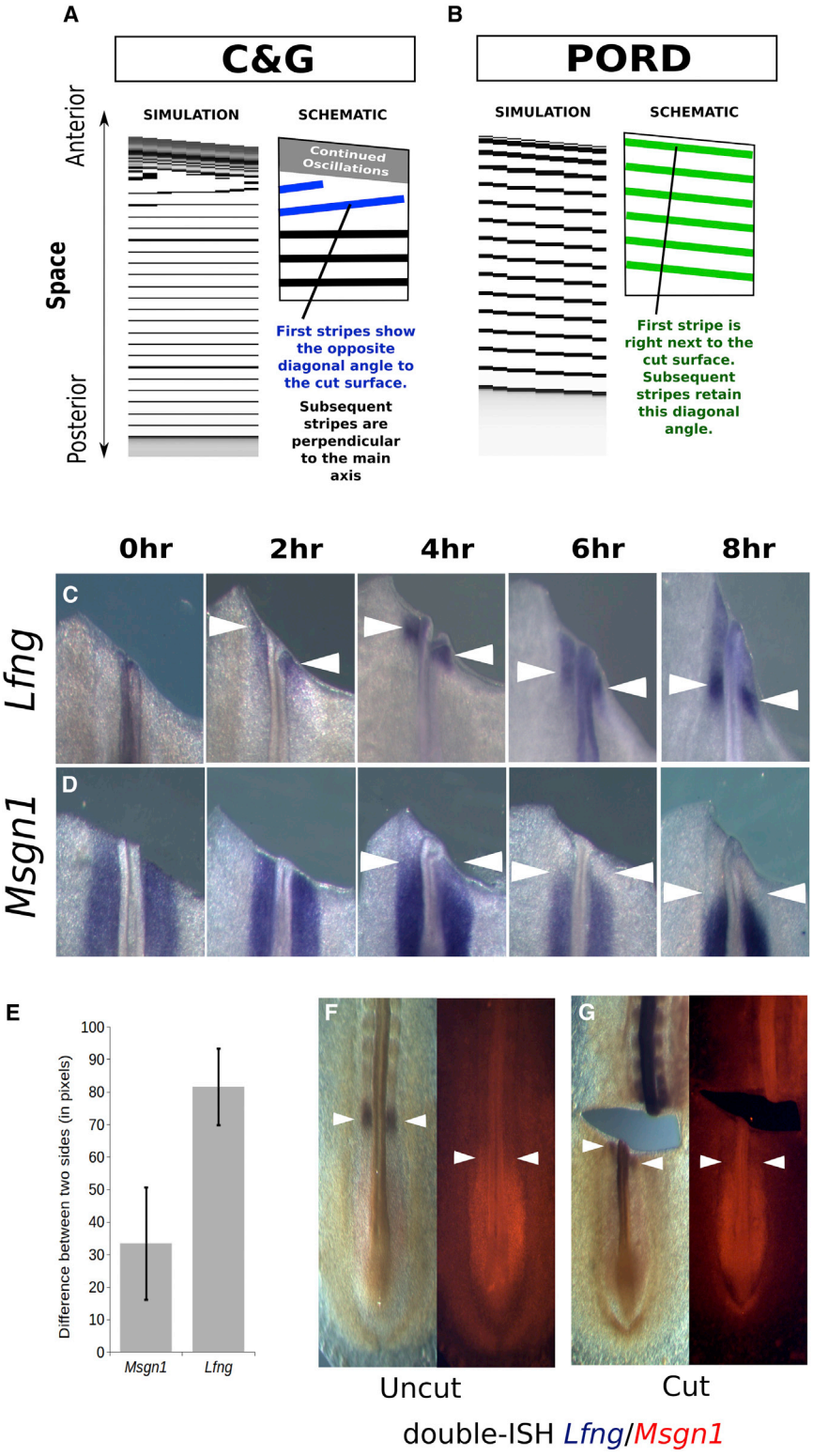

Figure 4. Decoupling the Progression of Segmental Patterning from the Progression of Global Gradients by Diagonal PSM Cuts

(A and B) Alternative model predictions generated by simulation. Pseudo 2D plots are generated by simulating either model with the tailbud position set in ten different positions in the range x = 240–250 (see Simulation Sheet 4). The C&G hypothesis predicts that the most stripes of *Lfng* or *Hairy1* will occur at specific positions along the AP axis, defined by the position of the long-range FGF/WNT gradients, and thus appear perpendicular to the primary axis. However, the first stripe or two (blue stripes) may not be perpendicular to the axis, but neither are they parallel to the cut edge. Instead, they will have the tendency to be at an angle opposite to the cut surface (and may be truncated because of this). In contrast, our PORD model predicts diagonal stripes (green) directly adjacent to the cut surface, irrespective of the AP position.

(C) The first stripe of *Lfng* expression appears exactly at the cut surface (~2–4 hr) and the second with a similar diagonal angle (~6–8 hr).

(D) However, the boundary of the FGF/WNT read out gene *Msgn1* moves continuously posteriorly without an asymmetry on either side of the embryo. White arrowheads indicate the diagonal expression patterns of *Lfng* and the symmetrical expression boundary of *Msgn1*.

(E) Quantification of the difference in the positions of the *Msgn1* expression boundary position and *Lfng* stripe between the two sides of the embryo (n = 12 for each group, t = 4-, 6-, and 8-hr time points combined), with SE.

(F and G) Double in situ hybridizations of *Lfng* and *Msgn1* in the same embryo act as an internal control and confirm that this result is not due to tissue deformation (n = 18/20 for observed precocious stripes).

such a manipulation is performed (see simulations in Figures 4A and 4B).

The C&G mechanism predicts that the positions of most somitic boundaries are relatively unaffected since cells are performing their segmentation program in response to global gradients (Figure 4A; most stripes are horizontal). However, it also predicts that the most anterior stripe will be slightly asymmetrical, but the opposite angle to that of the cut (Figure 4A). This is because the new wound-induced gradient of signaling (see Figure 3B) boosts the normal gradient, causing the arrest front to be more anterior on the shorter cut side of the PSM (right-hand side of cut in Figure 4A). Furthermore, high FGF signaling directly adjacent to the cut prevents cells from exiting oscillations predicting a zone of continued oscillations. The PORD mechanism by contrast predicts that the cut site locally seeds the formation of new stripes. These are also asymmetric, but parallel to the cut surface; hence, they have the opposite angle to the prediction of the C&G model (Figure 4B). Another difference between the predictions is that the

stripes from the PORD model will continue to be asymmetrical posteriorly along the PSM for a number of stripes (and will slowly reorient to become symmetrical, depending on the parameter values).

We first examined the impact of this experiment on stripe formation, as revealed by a time course of *Lfng* expression. Figure 4C shows that the first stripe formed (by 4 hr after the cut) is not perpendicular to the primary axis (horizontal), but instead displays a diagonal angle, running adjacent to the diagonal cut edge. The second stripe to form (8 hr) still displays a similar angle, thus suggesting support of the PORD model. To test whether the C&G mechanism could explain the diagonal stripes, we analyzed the dynamics of the large-scale gradient (revealed by *Msgn1* expression) during the cut experiment to see whether its movement is also affected by the diagonal cut. In contrast to stripe formation, the time course of *Msgn1* expression showed that the boundary moves at WT velocity throughout the incubation, as if the tissue had never been cut (Figure 4D). Although small differences were sometimes seen between the left and right side of the embryo, it was not enough to explain the dramatic asymmetries of the Lfng stripes (n = 12; Figures 4E and S4A). This discrepancy between the horizontal gradient readout and the diagonal stripes was also confirmed by double in situs within the same embryos (Figures 4F and 4G). We also confirmed this result by analyzing *Hairy* as an alternative to *Lfng*, and examining physical somite formation, which also displays the asymmetry (see Figure S4 for supplemental results and further controls). In summary, the best known molecular indicator of the gradient cannot explain the positions of stripes as a function of the C&G model, while the predictions of the PORD model are indeed observed in this experiment.

Long-Term Inhibition of FGF Signaling Supports a PORD Mechanism

Models that are mechanistically distinct may make similar predictions for certain perturbation experiments. Short-term inhibition of FGF signaling by SU5402 generates a single larger somite (Dubrulle et al., 2001; Sawada et al., 2001), but this result is predicted by both the C&G and PORD models (see Figure 1B for the C&G prediction). To find predictions that would differentiate between the models, we considered long-term inhibition experiments. SU5402 has a rapid impact on FGF signaling (Mohammadi et al., 1997) and somite patterning (Dubrulle et al., 2001), so signaling levels will reach maximal obtainable levels of repression very quickly, with that repression fading as the drug is metabolized. If the dose employed does not affect tail bud extension, then FGF signaling levels over the entire PSM will show a biphasic response (Figure 5A). In the first short phase, FGF signaling will be actively reduced, causing an effective posterior jump in the gradient velocity. In the second phase, repression of FGF will have reached saturating levels, and the gradient velocity will thus again match the normal speed of tailbud elongation, or even slow down if repression fades. The two models make very different predictions about the resulting somites from this experiment (Figure 5B and Movie S6 for PORD and Movie S7 for C&G). In the C&G model, movement of the arrest front is coupled to the movement of the FGF gradient. The somite that is patterned during the rapid posterior jump of the arrest front would be larger than normal. However, somites patterned during the second phase should be of normal size (or smaller than normal if the SU5402 starts to wear off). In contrast, our PORD model has no direct coupling between the long-range gradients and the arrest front. Simulations show that at the moment of treatment with SU5402, the velocity of the arrest front will not rapidly jump posteriorly, but will just increase moderately and then be maintained for the remainder of the experiment, creating multiple large somites.

Before testing these predictions, we had to perform control experiments to confirm that the long-range gradients respond in the biphasic manner expected. We incubated HH9-HH12 embryos for 12 hr with a single high dose of the FGF signaling inhibitor SU5402, which was not washed out during the course of the experiment. The spatiotemporal profile of *Msgn1* (Figures 5C and 5D) confirmed that rapid repression is already achieved by 3 hr, at which point the signaling gradient has moved posteriorly by more than a somite length (corresponding to phase 1 in Figure 5A). The time course also confirmed that roughly the same level of repression is maintained for the remaining 6 hr since the relative difference in position of the *Msgn1* expression boundary between the SU5402 and control embryos remains relatively constant (corresponding to phase 2 in Figure 5A). Thus, the expected biphasic response to SU5402 is confirmed: a rapid and dramatic impact on signaling, followed by a long equilibrium phase in which the posterior velocity reverts back to its normal speed (flat region in Figure 5D). The rapid reduction in FGF/WNT signaling result was further confirmed by qPCR of cDNA from the FGF signaling readout genes *Dusp6* and *Pea3* at different time points in the PSM (Figure 5E).

To test whether the resulting phenotype supports either the PORD or the C&G mechanism, we analyzed physical somites after 12 hr of FGF repression (as *Lfng* expression does not last long enough to record the history of multiple somites). The delay between molecular stripe formation and physical somite patterning means that larger somites are not seen until three normal ones have formed (hence the difference between the dashed and solid lines in Figure 5B). Nevertheless, once larger somites are seen, instead of just one or two large somites, as predicted by the C&G model, we consistently observed multiple large somites (Figures 5F and 5G). In principle, larger somites could be the result of a higher velocity of the arrest front, or a slower clock. To test the latter possibility, we counted the number of somites formed during the experiment and compared them with control embryos. No significant difference was seen between the two groups (an average of 4.7 for controls versus 5.0 for inhibited, n = 10; Figure 5H). In contrast, it was clear that the arrest front had moved with a higher velocity, as the last formed somite boundary was more posterior in treated embryos after 12 hr (compare white arrowheads in Figure 5F). These results show that the real arrest front moved at a moderately higher velocity (~40% faster) during most of the experiment. This contrasts with the FGF gradient, which initially jumped by more than a somite (compare white arrowheads in Figure 5C, which indicate more than a doubling of velocity over the first 3 hr) but then continued to progress at normal speed (Figure 5D). To complete the analysis, we also tested a modified version of the C&G model to show that adding a delay between FGF signaling and the downstream network is not sufficient to make it fit the observed results (Figure S5; Movie S8).

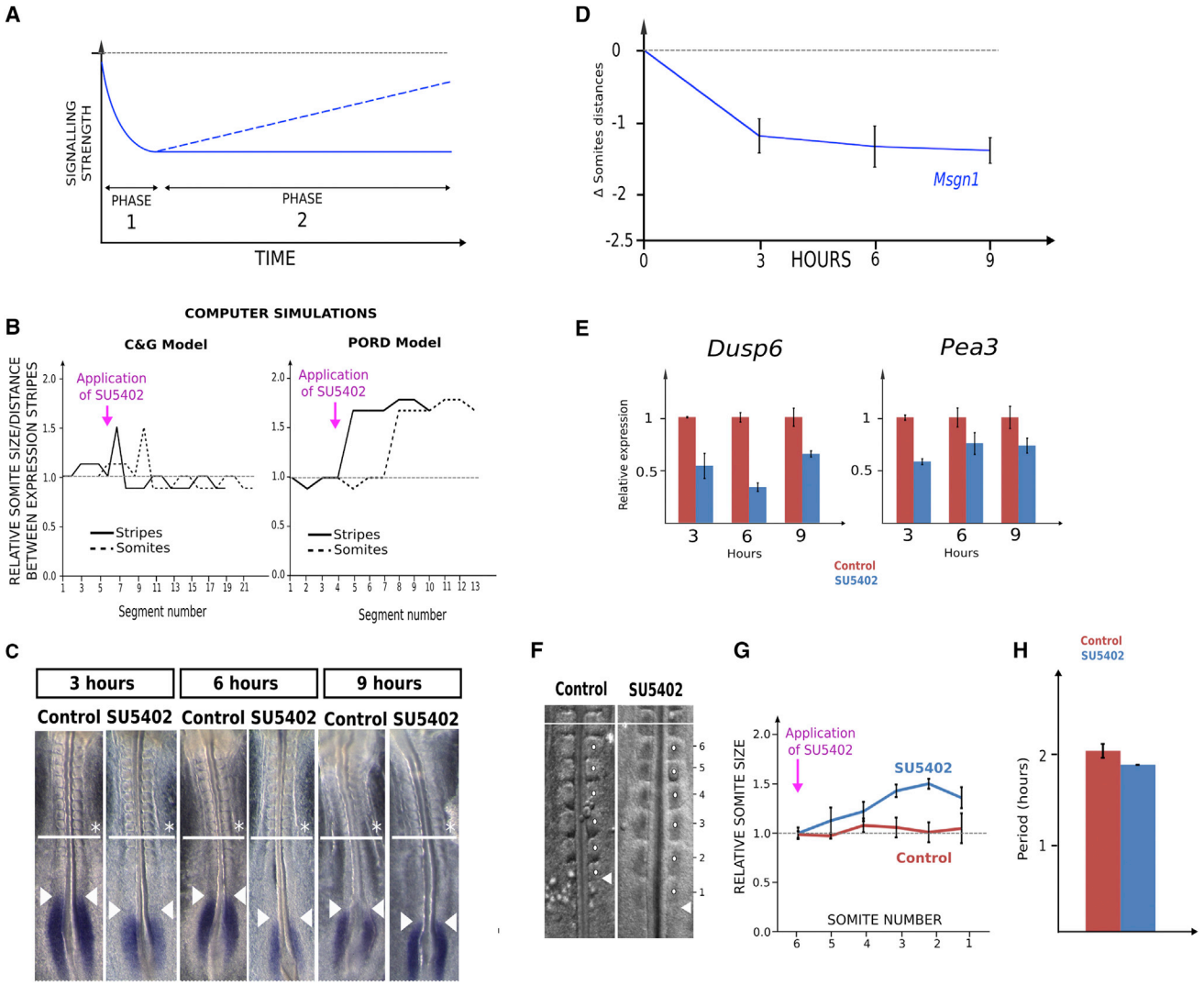

Figure 5. Long-Term Inhibition of FGF Signaling Supports the PORD Mechanism

(A) Expected dynamics of FGF signaling in response to repression by SU5402. The rapid repression (phase 1) is followed either by stable reduced signaling (solid line) or a gradual recovery to normal levels (dashed line).

(B) Contrasting predictions of the C&G hypothesis versus the PORD model: in the first case, the rapid posterior shift of the FGF gradient causes a transient acceleration of the arrest front and a large somite. However, once a stable repressed level of FGF signaling has been reached (phase 2), the velocity reverts to normal, and subsequent somites are of normal size. In contrast, in the PORD model, the FGF gradient and arrest front are not directly linked, and a different outcome is predicted for the same virtual SU5402 experiment. The globally reduced FGF levels result in larger buffer zones and thus multiple large somites. The velocity of the emergent arrest front is also increased. The time of application of the drug treatment is shown with a purple arrow. Main predictions of the models (distances between stripes of gene expression) are shown with a solid line. The dashed line shows the expected distribution of somite sizes, which is a morphogenetic event observable about three segments later than the molecular pattern of stripes (i.e., when SU5402 treatment is performed, two to three unformed somites are already molecularly patterned).

(C) In situ hybridizations of the *Msgn1* gene revealed that after just 3 hr its anterior expression boundary has jumped posteriorly with respect to a control embryo (compare white arrowheads). However, this shift does not increase over time, but rather is maintained at a similar level during the rest of the experiment (6 and 9 hr). An asterisk and white line marks the last formed somite prior to the experiment.

(D) Quantification of the shifted expression boundary from (C). The shift (in somite lengths) is plotted for each time point (plus SE bars), supporting the expected bi-phasic response illustrated in (B).

(E) qPCR to detect mRNA levels of the FGF signaling readout genes *Dusp6* and *Pea3* confirms the result obtained with *Msgn1* in situ. SE is plotted.

(F) SU5402 causes multiple large somites, which are quantified in (G) (n = 5 and 4 for test and control, respectively). SE is plotted. Following convention, numbering starts with the last-formed somite.

(H) The period time is not significantly different between tests and controls. Period is measured as the time of the incubation divided by the number of somites generated during incubation. SE is plotted.

DISCUSSION

Nearly 4 decades after the clock and wavefront model was first proposed, one of its core concepts still plays a prominent role in current models of somite patterning. Namely, the precise posterior movement of the arrest front, which is responsible for converting temporal oscillations into a highly regular spatial periodic pattern, is controlled by long-range positional information. This idea still lies at the heart of the more recent molecularly based C&G models. An inescapable prediction of this idea is that any deviation in velocity of this wavefront will cause irregularities in the periodic spacing of the molecular prepattern (and the subsequent sizes of somites), and yet, although it is unclear how such a long-range gradient could provide such positional precision when traveling through the PSM, somite patterning is highly regular.

Here, we have performed an unbiased theoretical re-evaluation of the possible models that could explain progressive, periodic somite patterning. We have found an alternative theoretical model that is fundamentally different to the prevailing C&G model and does not rely on positional information provided by long-range FGF/WNT gradients to create a periodic pattern of expression stripes (see Movie S4). Although in this manuscript we focus on the specific PORD mechanism that was identified in our computational screen, the PORD and C&G models are just examples representing the primary dichotomy in the field of pattern formation mechanisms—namely local self-organizing RD and long-range positional information (Green and Sharpe, 2015). Our goal therefore has been to reveal that a RD model is capable of explaining the vast majority of known observations and even more that most of these observations are easier to explain with RD than with positional information.

On the experimental side, a key goal was to demonstrate a lack of coupling between the gradient and the arrest front. We have shown this in two complementary ways: both by (1) perturbing the velocity of the determination front without altering the gradient velocity and conversely by (2) changing the velocity of the gradient without causing a similar change in the velocity of the determination front. The former (1) was demonstrated by performing physical cuts in the PSM (both straight and diagonal cuts), which cause a shift (both in time and space) in the stripe-forming program of *Lfng* (Figures 3E, 3F, and 4C) and which yet have no impact on movement of the main FGF/WNT gradient (Figure 4D). Our discovery of induced FGF signaling in these cut experiments also questioned the interpretation of previous similar experiments, which had concluded that a progressive "relay" mechanism could not be involved. The latter (2) we demonstrated by pharmacological inhibition of FGF signaling. The dynamics of the posteriorly traveling gradient changed dramatically, while the velocity of the arrest front (as visualized both by *Lfng* expression, and morphological somite formation) only experienced a smooth, prolonged, and mild increase in speed (Figure 5).

By decoupling the determination front from the FGF/WNT gradients, we have shown that somite size (distance between adjacent expression stripes) is not causally determined by the speed at which these signaling gradients move through the PSM. Instead, we propose that the primary determinants of somite size are local and based on diffusion from the last-formed stripe. Indeed, Cooke and Zeeman (1976) also recognized that a local self-organizing Turing mechanism could produce a progressive periodic pattern and that a traveling wavefront could still be observed in this scenario. For this reason, they emphasized that despite the name "clock and wavefront model" the distinguishing feature of their hypothesis was a "necessary relation" with positional information—not the presence of a clock or a wavefront per se (indeed, our PORD model also involves oscillations and an emergent wavefront, but is fundamentally different to the C&W model). Their explicit discussion of the Turing model highlights that our PORD model is in fact the revival of an old idea. However, our version displays three clear improvements over previous versions. First, our PORD model is an explicit network-based mathematical model, which can be simulated and whose dynamical behavior can be examined in detail, while in contrast Cooke and Zeeman (1976) considered this option only in general abstract terms. Second, the ability to simulate our model has allowed us to discover that the original concerns about RD models are completely overcome by our PORD model. Specifically, our PORD model can indeed produce (1) scaling of somite size in relation to PSM growth rates and (2) also supports cell-autonomous oscillations.

Third, although our model displays all the features contained in its name—PORD model—further simulations reveal that changing just single parameter values is sufficient to lose the progressive and oscillatory aspects, leaving a RD system that is capable of spontaneous segmentation (see Supplemental Information, Data S1). This may explain three intriguing observations: (1) the recent demonstration of simultaneous segmentation in culture experiments (Dias et al., 2014), (2) the observation that the anterior-most somites of normal embryos also form simultaneously, and (3) the fact that even in the absence of most FGF signaling the embryo still manages to create up to 10 somites, which are disorganized (Naiche et al., 2011). Our model thus displays an advantage over another mathematical model, which also recently proposed that the arrest front is an emergent local phenomenon (Murray et al., 2011). The Murray model is based on abstract coupled oscillators (rather than reacting and diffusing molecules) and is thus incapable of switching into this observed non-progressive/simultaneous mode.

A detailed discussion of other benefits of the PORD model is beyond the scope of this paper, but we briefly highlight that it is able to explain (1) the divergent definitions in the literature of the determination front (Dubrulle et al., 2001) compared to the arrest front, illustrated by performing virtual tissue inversion experiments (Supplemental Information, Data S2; Movies S9 and S10), (2) multiple waves of expression in snakes (Movie S11), (3) phase-gradient encoding, and (4) the impact of retinoic acid treatment (see Supplemental Information, Data S3, S4 and S5).

Our proposal does not reject the idea that traveling gradients of FGF and WNT signaling control the timing of the physical budding process of somitogenesis. Here a distinction must be made between the upstream molecular patterning process (addressed by the PORD model) and the subsequent morphogenetic activities. Although we were able to induce precocious stripes of Lfng (posterior to their normal position), we did not see precocious physical somites, suggesting that the timing of the subsequent mesenchymal-to-epithelial transitions may indeed be controlled by the long-range gradients.

In summary, early theoretical work on somite patterning considered both local self-organizing processes as well as long-range positional information. However, during the last couple of decades, the concepts of long-range gradients and global positional specification of the arrest front have dominated the field. Here we propose a theoretical model, which is fundamentally different from the C&G model and makes experimentally testable predictions. Our experimental analysis has revealed that the evidence supporting our PORD model rivals the evidence for a global positional-information mechanism. The PORD model is particularly interesting at a theoretical level. Although the stripe-forming behavior is essentially a local Turing system and does not depend on global positional information, nevertheless we show that modulation of this reaction-diffusion system by global FGF/WNT gradients may allow scaling of somites in relation to embryo size. As such this would be another example of a local self-organizing process collaborating with long-range gradients to afford precision, scaling and robustness to developmental patterning.

EXPERIMENTAL PROCEDURES

Implementation of the Model

The basic model that we implemented to explore the design space for topologies capable of segmentation was the same as that previously described (Cotterell and Sharpe, 2010). However, to adapt the model so that it was suitable for exploring a design space of somitogenesis, we made five changes that are described comprehensively in the Supplemental Experimental Procedures, along with details of our simulations.

In Vivo Experiments

Standard chick explant, qPCR, immunofluorescence, and in situ hybridization protocols were used; details can be found in the Supplemental Experimental Procedures. Likewise, FGF-inhibition and PSM-cut experiments are described comprehensively in the Supplemental Experimental Procedures.

SUPPLEMENTAL INFORMATION

Supplemental Information includes Supplemental Experimental Procedures, five figures, five data files, and eleven movies and can be found with this article online at http://dx.doi.org/10.1016/j.cels.2015.10.002.

ACKNOWLEDGMENTS

We acknowledge support of the Spanish Ministry of Economy and Competitiveness, "Centro de Excelencia Severo Ochoa 2013-2017," SEV-2012-0208.

Received: August 21, 2015
Revised: September 11, 2015
Accepted: October 7, 2015
Published: October 28, 2015

REFERENCES

Aulehla, A., and Johnson, R.L. (1999). Dynamic expression of lunatic fringe suggests a link between notch signaling and an autonomous cellular oscillator driving somite segmentation. Dev. Biol. *207*, 49–61.

Aulehla, A., Wehrle, C., Brand-Saberi, B., Kemler, R., Gossler, A., Kanzler, B., and Herrmann, B.G. (2003). Wnt3a plays a major role in the segmentation clock controlling somitogenesis. Dev. Cell *4*, 395–406.

Baker, R.E., Schnell, S., and Maini, P.K. (2006a). A mathematical investigation of a Clock and Wavefront model for somitogenesis. J. Math. Biol. *52*, 458–482.

Baker, R.E., Schnell, S., and Maini, P.K. (2006b). A clock and wavefront mechanism for somite formation. Dev. Biol. *293*, 116–126.

Bessho, Y., Miyoshi, G., Sakata, R., and Kageyama, R. (2001a). Hes7: a bHLH-type repressor gene regulated by Notch and expressed in the presomitic mesoderm. Genes Cells *6*, 175–185.

Bessho, Y., Sakata, R., Komatsu, S., Shiota, K., Yamada, S., and Kageyama, R. (2001b). Dynamic expression and essential functions of Hes7 in somite segmentation. Genes Dev. *15*, 2642–2647.

Cooke, J. (1975). Control of somite number during morphogenesis of a vertebrate, Xenopus laevis. Nature *254*, 196–199.

Cooke, J., and Zeeman, E.C. (1976). A clock and wavefront model for control of the number of repeated structures during animal morphogenesis. J. Theor. Biol. *58*, 455–476.

Cotterell, J., and Sharpe, J. (2010). An atlas of gene regulatory networks reveals multiple three-gene mechanisms for interpreting morphogen gradients. Mol. Syst. Biol. *6*, 425.

Deuchar, E.M., and Burgess, A.M.C. (1967). Somite segmentation in amphibian embryos: is there a transmitted control mechanism? J. Embryol. Exp. Morphol. *17*, 349–358.

Dias, A.S., de Almeida, I., Belmonte, J.M., Glazier, J.A., and Stern, C.D. (2014). Somites without a clock. Science *343*, 791–795.

Dubrulle, J., and Pourquié, O. (2004). fgf8 mRNA decay establishes a gradient that couples axial elongation to patterning in the vertebrate embryo. Nature *427*, 419–422.

Dubrulle, J., McGrew, M.J., and Pourquié, O. (2001). FGF signaling controls somite boundary position and regulates segmentation clock control of spatiotemporal Hox gene activation. Cell *106*, 219–232.

Forsberg, H., Crozet, F., and Brown, N.A. (1998). Waves of mouse Lunatic fringe expression, in four-hour cycles at two-hour intervals, precede somite boundary formation. Curr. Biol. *8*, 1027–1030.

François, P., Hakim, V., and Siggia, E.D. (2007). Deriving structure from evolution: metazoan segmentation. Mol. Syst. Biol. *3*, 154.

Gomez, C., Ozbudak, E.M., Wunderlich, J., Baumann, D., Lewis, J., and Pourquié, O. (2008). Control of segment number in vertebrate embryos. Nature *454*, 335–339.

Green, J.B., and Sharpe, J. (2015). Positional information and reaction-diffusion: two big ideas in developmental biology combine. Development *142*, 1203–1211.

Herrgen, L., Ares, S., Morelli, L.G., Schröter, C., Jülicher, F., and Oates, A.C. (2010). Intercellular coupling regulates the period of the segmentation clock. Curr. Biol. *20*, 1244–1253.

Hester, S.D., Belmonte, J.M., Gens, J.S., Clendenon, S.G., and Glazier, J.A. (2011). A multi-cell, multi-scale model of vertebrate segmentation and somite formation. PLoS Comput. Biol. *7*, e1002155.

Holley, S.A., Geisler, R., and Nüsslein-Volhard, C. (2000). Control of her1 expression during zebrafish somitogenesis by a delta-dependent oscillator and an independent wave-front activity. Genes Dev. *14*, 1678–1690.

Ishihara, S., and Kaneko, K. (2006). Turing pattern with proportion preservation. J. Theor. Biol. *238*, 683–693.

Jiang, Y.-J., Aerne, B.L., Smithers, L., Haddon, C., Ish-Horowicz, D., and Lewis, J. (2000). Notch signalling and the synchronization of the somite segmentation clock. Nature *408*, 475–479.

Jouve, C., Palmeirim, I., Henrique, D., Beckers, J., Gossler, A., Ish-Horowicz, D., and Pourquié, O. (2000). Notch signalling is required for cyclic expression of the hairy-like gene HES1 in the presomitic mesoderm. Development *127*, 1421–1429.

Kondo, S., and Miura, T. (2010). Reaction-diffusion model as a framework for understanding biological pattern formation. Science *329*, 1616–1620.

Kulesa, P.M., Schnell, S., Rudloff, S., Baker, R.E., and Maini, P.K. (2007). From segment to somite: segmentation to epithelialization analyzed within quantitative frameworks. Dev. Dyn. *236*, 1392–1402.

Lin, G., and Slack, J.M. (2008). Requirement for Wnt and FGF signaling in Xenopus tadpole tail regeneration. Dev. Biol. *316*, 323–335.

Maroto, M., Dale, J.K., Dequéant, M.L., Petit, A.C., and Pourquié, O. (2005). Synchronised cycling gene oscillations in presomitic mesoderm cells require cell-cell contact. Int. J. Dev. Biol. *49*, 309–315.

McGrew, M.J., Dale, J.K., Fraboulet, S., and Pourquié, O. (1998). The lunatic fringe gene is a target of the molecular clock linked to somite segmentation in avian embryos. Curr. Biol. *8*, 979–982.

Meinhardt, H. (1982). Models of Biological Pattern Formation (Academic Press).

Mohammadi, M., McMahon, G., Sun, L., Tang, C., Hirth, P., Yeh, B.K., Hubbard, S.R., and Schlessinger, J. (1997). Structures of the tyrosine kinase domain of fibroblast growth factor receptor in complex with inhibitors. Science *276*, 955–960.

Murray, P.J., Maini, P.K., and Baker, R.E. (2011). The clock and wavefront model revisited. J. Theor. Biol. *283*, 227–238.

Naiche, L.A., Holder, N., and Lewandoski, M. (2011). FGF4 and FGF8 comprise the wavefront activity that controls somitogenesis. Proc. Natl. Acad. Sci. USA *108*, 4018–4023.

Oates, A.C., and Ho, R.K. (2002). Hairy/E(spl)-related (Her) genes are central components of the segmentation oscillator and display redundancy with the Delta/Notch signaling pathway in the formation of anterior segmental boundaries in the zebrafish. Development *129*, 2929–2946.

Packard, D.S., Jr. (1978). Chick somite determination: the role of factors in young somites and the segmental plate. J. Exp. Zool. *203*, 295–306.

Packard, D.S., Jr., and Jacobson, A.G. (1976). The influence of axial structures on chick somite formation. Dev. Biol. *53*, 36–48.

Palmeirim, I., Henrique, D., Ish-Horowicz, D., and Pourquié, O. (1997). Avian hairy gene expression identifies a molecular clock linked to vertebrate segmentation and somitogenesis. Cell *91*, 639–648.

Pearson, M., and Elsdale, T. (1979). Somitogenesis in amphibian embryos. I. Experimental evidence for an interaction between two temporal factors in the specification of somite pattern. J. Embryol. Exp. Morphol. *51*, 27–50.

Sawada, A., Fritz, A., Jiang, Y.J., Yamamoto, A., Yamasu, K., Kuroiwa, A., Saga, Y., and Takeda, H. (2000). Zebrafish Mesp family genes, mesp-a and mesp-b are segmentally expressed in the presomitic mesoderm, and Mesp-b confers the anterior identity to the developing somites. Development *127*, 1691–1702.

Sawada, A., Shinya, M., Jiang, Y.J., Kawakami, A., Kuroiwa, A., and Takeda, H. (2001). Fgf/MAPK signalling is a crucial positional cue in somite boundary formation. Development *128*, 4873–4880.

Tiedemann, H.B., Schneltzer, E., Zeiser, S., Hoesel, B., Beckers, J., Przemeck, G.K.H., and de Angelis, M.H. (2012). From dynamic expression patterns to boundary formation in the presomitic mesoderm. PLoS Comput. Biol. *8*, e1002586.

Turing, A.M. (1952). The chemical basis of morphogenesis. *Phil Trans Royal Soc Lon*. Series B. Biol. Sci. *641*, 37–72.

Whitehead, G.G., Makino, S., Lien, C.L., and Keating, M.T. (2005). fgf20 is essential for initiating zebrafish fin regeneration. Science *310*, 1957–1960.